

Review

Not peer-reviewed version

---

# Laser Cavitation Peening: A Review

---

[Hitoshi Soyama](#)<sup>\*</sup> and Yuka Iga

Posted Date: 27 April 2023

doi: 10.20944/preprints202304.1006.v1

Keywords: pulsed laser; cavitation; mechanical surface treatment; cavitation peening; additive manufactured metal; fatigue strength; titanium alloy



Preprints.org is a free multidiscipline platform providing preprint service that is dedicated to making early versions of research outputs permanently available and citable. Preprints posted at Preprints.org appear in Web of Science, Crossref, Google Scholar, Scilit, Europe PMC.

Copyright: This is an open access article distributed under the Creative Commons Attribution License which permits unrestricted use, distribution, and reproduction in any medium, provided the original work is properly cited.

*Review*

# Laser Cavitation Peening: A Review

**Hitoshi Soyama <sup>1,\*</sup> and Yuka Iga <sup>2</sup>**<sup>1</sup> Department of Finemechanics, Tohoku University, Sendai 980-8579, Japan<sup>2</sup> Institute of Fluid Science, Tohoku University, Sendai 980-8577, Japan

\* Correspondence: soyama@mm.mech.tohoku.ac.jp; Tel.: +81-22-795-6891; Fax.: +81-22-795-3758

**Featured application: laser cavitation peening can be applied to enhance the fatigue strength of metallic materials, including three-dimensional additively manufactured metals (3D metals).**

**Abstract:** During submerged laser peening using a pulsed laser, a bubble that behaves like cavitation is generated after laser ablation (LA). The bubble is referred to as laser cavitation (LC). The amplitude of the shock-wave in LA water is larger than that of LC; however, the impact passing through the target metal during LC is larger than that of LA. Thus, submerged laser peening is referred to as “laser cavitation peening”, as the peening method using the cavitation impact is known as “cavitation peening”. The impact induced by a hemispherical bubble is more aggressive than that of a spherical bubble with a microjet. Laser cavitation peening can improve the fatigue strength of metallic materials by producing work-hardening and the introduction of compressive residual stress. Three-dimensional additive manufactured metals (3D metals) such as titanium alloy are attractive materials for aviation components and medical implants; however, the fatigue strength of as-built components is nearly half that of bulk metals, and this is an obstacle for the applications of 3D metals. In the present study, published research papers were reviewed to identify the key factors of laser cavitation peening, with additional visualization of LC and data. Then, improvements in the fatigue strength of metallic materials, including 3D metals produced by laser cavitation peening, were summarized.

**Keywords:** pulsed laser; cavitation; mechanical surface treatment; cavitation peening; additive manufactured metal; fatigue strength; titanium alloy

---

## 1. Introduction

In order to establish a sustainable society, improvements in the life and reliability of machine components are required to save energy and resources. Mechanical surface treatments such as shot peening comprise one of most powerful methods to increase fatigue life and strength [1]. In addition, three-dimensional additively manufactured metallic materials (3D metals) are attractive metals for medical implants [2] and aviation components [3], as the components are directly formed from CAD/CAM data. However, the fatigue strength of 3D metals is almost half that of wrought metals [3], and improving the fatigue strength of 3D metals is a serious issue in respect of their practical use. Laser peening [4,5] and cavitation peening [6] are newly developed methods used to improve the fatigue properties of metallic materials. One of the reasons for the weak fatigue strength of 3D metals is their extremely large surface roughness due to unmelted metal particles on the surface. As laser ablation smoothens the surface of 3D metals and laser shock introduces compressive residual stress and work hardening, laser peening can improve the fatigue properties of metallic materials, including 3D metals [7–10].

In respect of laser peening, also known as laser shock peening, there are three methods. In the first method, a pulsed laser is irradiated to a target surface that is covered with a water film [4]. In the second method, the target is placed in water and a pulsed laser is applied to the target surface, i.e., submerged laser peening [11]. In these two types of laser peening, water or a confinement layer [12] is required. In the third method, dry laser peening is carried out without a confinement layer using a femtosecond pulsed laser [13,14]. For all three laser-peening methods, including submerged

laser peening, it has been hypothesized that the peening mechanism that introduces local plastic deformation on the metal surface is caused by laser ablation [15]. Namely, it is thought that the inertial force caused by the shock-wave is contained by the water, and this produces plastic deformation in metallic materials [4,15]. In the case of submerged laser peening, a bubble that behaves like a cavitation bubble is generated after laser ablation, and this is known as laser cavitation [16,17]. In previous studies, when the amplitude of the pressure wave in the water was measured using a shock-wave sensor that was placed in the water, the amplitude of laser ablation was larger than that of laser cavitation collapse [18–20]. However, in another study, when the impact force passing through the target metal was measured using an impact sensor with a polyvinylidene fluoride PVDF film [21], the impact during laser cavitation collapse was larger than that of laser ablation [16,19,20]. Cavitation bubble oscillation during submerged laser peening has also been investigated, and it was concluded that the first bubble oscillation was effective for the submerged laser peening [22]. The introduction of compressive residual stress and the work-hardening of aluminum alloy has also been demonstrated using laser cavitation [23]. These results reveal that laser cavitation impact can be utilized for peening.

Cavitation peening, in which cavitation bubble collapse impacts are used for peening, has been developed [6], and it has been applied for mitigation of the stress corrosion cracking of nuclear power plants [24]; there are also reports that show improvements in the fatigue strength of metallic materials, including 3D metals [6]. In the case of conventional cavitation peening, cavitation is generated by injecting a high-speed water jet into water, i.e., a cavitating jet [6]. The peening mechanism using a cavitating jet is different from that of water jet peening, in which water-column impacts are used for peening [25]. The peening intensity using a cavitating jet under optimum conditions was shown to be more effective than that of a water jet [6]. Namely, it is worthwhile to use the impact at cavitation collapse for peening. As mentioned above, as submerged laser peening can use the impact of the laser cavitation collapse, it is a type of cavitation peening that uses laser cavitation [6]. Therefore, it can be referred to as laser cavitation peening.

The collapse of a spherical cavitation bubble near a solid boundary in water was computed by Plesset and Chapman [26] (see Figure 1), and then the deformation of the bubble was experimentally observed using high-speed photography at a framing rate of 300,000 frames/s [27]. A microjet in a cavitation bubble was also clearly identified by Crum [28]. Microjets and shock-waves have been attractive phenomena for researchers and engineers, and are important for understanding bubble dynamics [29] and sonochemistry [30]. The microjet in a cavitation bubble is still an attractive phenomenon for researchers [31–34]. As shown in Figure 1, the development of the microjet in the spherical cavitation bubble is an interesting phenomenon, and some researchers believe that the microjet during cavitation bubble collapse can be utilized for peening. Actually, it has been demonstrated numerically, using fluid/material-coupled numerical simulations, that the pressure produced by the collapse of a hemispherical bubble is much stronger than that of microjet-type collapse, as shown in Figure 2 [35]. In Figure 2, the black line shows the shape of the bubble changing with time, and the color contour reveals the pressure in the fluid and the equivalent stress in the material at bubble collapse. Although the microjet during the bubble collapse generates a pressure wave of  $\approx 100$  MPa, the collapse of the hemispherical bubble produces pressure waves several times larger than that of the microjet. Thus, a hemispherical bubble should be used for laser cavitation peening. Note that the pressure induced by a flattened bubble, i.e., a pancake-type bubble, or a longitudinal bubble is weaker than that of a hemispherical bubble [35].

In order to use cavitation peening to enhance the fatigue properties of metallic materials, knowledge of fluid dynamics is required [6], as cavitation is a hydrodynamic phenomenon. Thus, in the present review, to clarify the mechanism of laser cavitation peening, the effectiveness of the laser cavitation impact for peening is explained using published papers, with additional observations in respect of laser cavitation. The effect of the bubble shape is discussed experimentally and numerically, and comparisons are made between a hemispherical bubble and a bubble with a microjet. Key factors in respect of laser cavitation peening are also summarized. Finally, improvements in the fatigue properties of metallic materials, including 3D metals, are demonstrated.

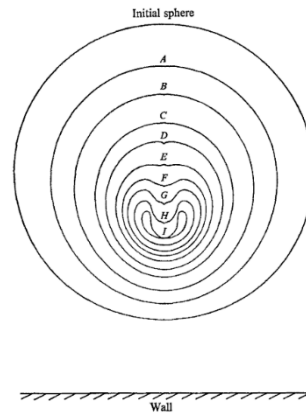


**Figure 1.** Collapse of a cavitation bubble near a solid boundary in water, computed by Plesset and Chapman. Reprinted from [26], with permission from Cambridge University Press, License Number 5517380575228.

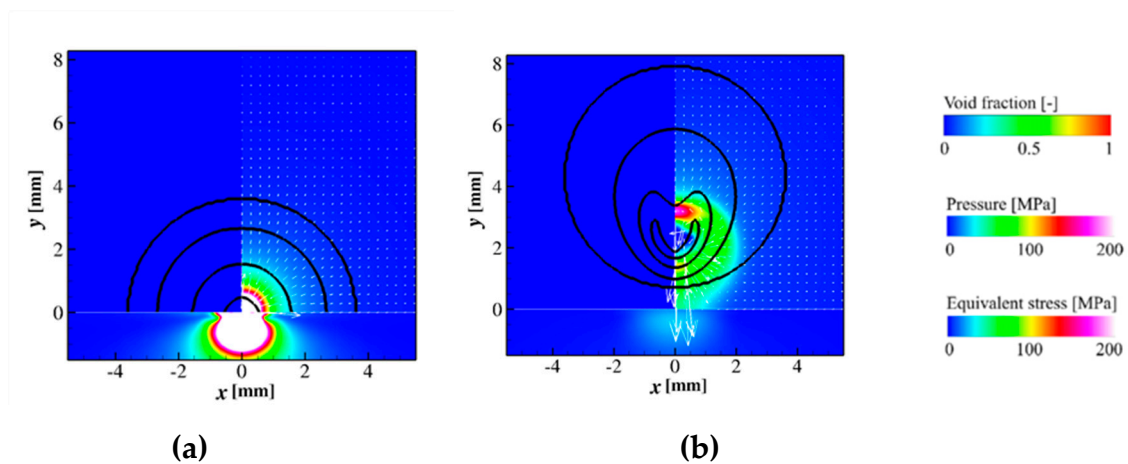


**Figure 2.** Fluid/material-coupled numerical simulation of collapse of a bubble near a wall, by Iga and Sasaki [35]: (a) spherical bubble near the wall (microjet mode); (b) hemispherical bubble on the wall (hemispherical mode).

## 2. Peening Using a Pulsed Laser

### 2.1. Laser Peening under Water (Laser Cavitation Peening) and Laser Peening with a Water Film

As described in the introduction, three peening methods using a pulse laser have been developed: laser peening under water [11,15–17,20], laser peening with a water film [4,12,36,37], and dry laser peening [13,14]. As shown in Figure 3, for both conventional laser peening under water and laser peening with a water film, it is thought that the inertial force of water confines the shock-wave generated by the plasma, which is caused by laser ablation, and produces local plastic deformation on the material surface. Normally, a sacrificial overlay such as paint or tape is used for laser peening with a water film, and this is not required for laser peening under water.

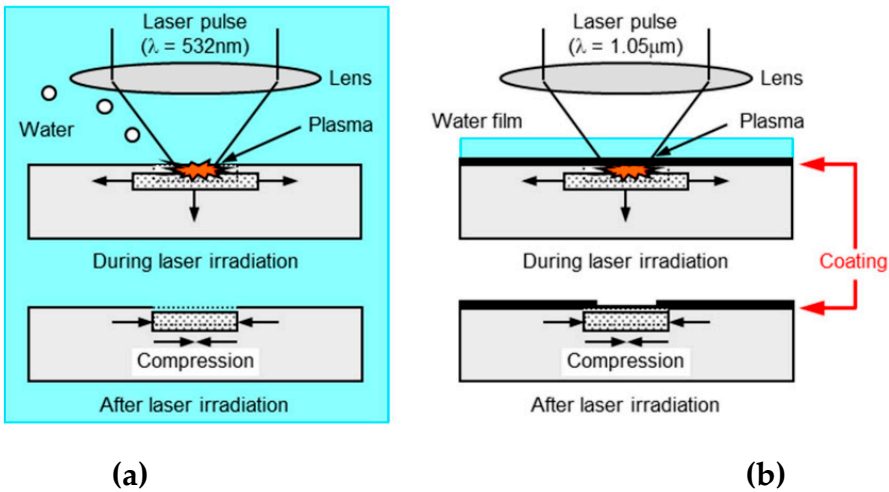


**Figure 3.** Fundamental process: (a) laser peening without coating (LPwC); (b) laser peening with coating (sacrificial overlay) [5].

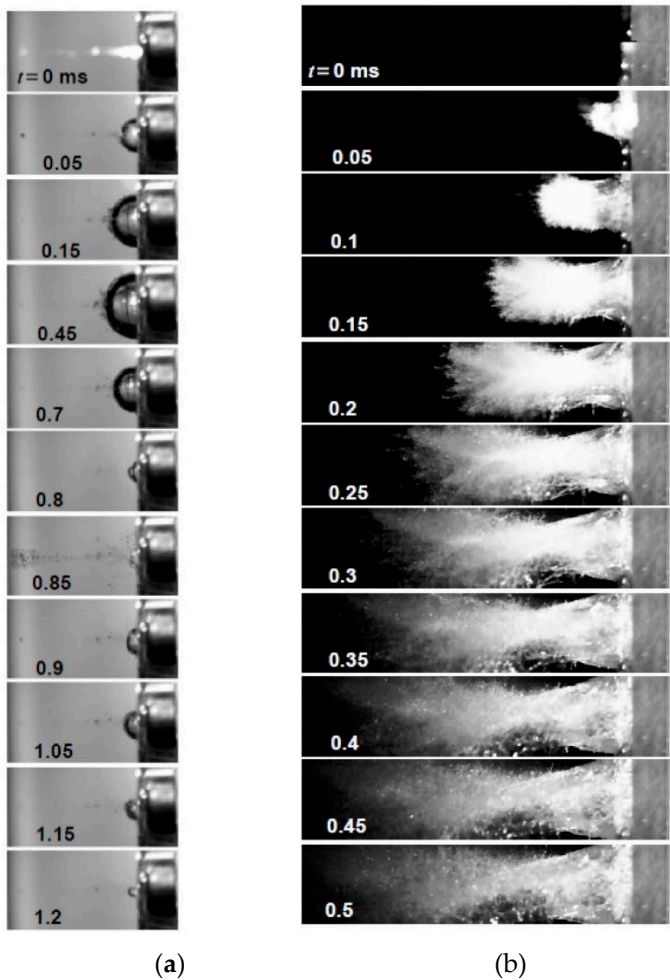


**Figure 4.** Images of laser peening: (a) laser peening under water (laser cavitation peening); (b) laser peening with a water film. Reprinted from [6] with permission from Elsevier, License Number 5532490457730.

Figure 4 shows images of laser peening for (a) laser peening under water (laser cavitation peening) and (b) laser peening with a water film [6]. In the case of laser peening with a water film, the water film was splashed away, as shown in Figure 4 (b). However, during laser peening under



water, a bubble was initiated after laser ablation ( $t = 0$  ms) and developed then collapsed ( $t = 0.85$  ms), as shown in Figure 4 (a). As the bubble was induced by a pulsed laser, this process is known as laser cavitation, and it behaves like a cavitation bubble. As mentioned later, the impact at collapse of the laser cavitation can be utilized for peening; the same situation applies for the laser ablation impact. Peening methods using laser cavitation are known as laser cavitation peening. The laser cavitation impact is larger than that of the laser ablation impact under optimized laser cavitation peening conditions.

## 2.2. Laser Cavitation Peening System

In order to illustrate laser cavitation peening systems, Figure 5 shows a schematic diagram of a laser cavitation peening test section. A target was placed in a water-filled glass chamber. A pulsed laser from a laser source was expanded using a concave lens, then focused on the target surface using convex lens(es) to avoid damage to the glass of the chamber. The standoff distances in air  $s_a$  and water  $s_w$  were optimized by measuring the peening intensity with  $s_a$  and  $s_w$ . During conventional submerged laser peening, the second harmonic of a Nd:YAG laser, i.e., a wavelength of 532 nm, is used in order to avoid absorption in the water [5]. However, from the point of view of the generation of cavitation bubbles, the fundamental harmonic, i.e., 1064 nm, is more beneficial, since the heat is more concentrated; researchers who have investigated cavitation bubbles using pulsed lasers have used Nd:YAG lasers [38]. A total of 40% of the pulse energy at 1064 nm is lost to obtain 532 nm during wavelength conversion. It was reported that the laser cavitation induced by a 1064 nm pulsed laser introduced compressive residual stress into hard metals such as alloy tool steel, when the standoff distance in water was optimized [39]. Recently, a portable submerged laser peening system using a pulsed laser with a wavelength of 1064 nm was developed [40]. In order to measure the pressure and/or impact caused by the laser ablation and laser cavitation collapse, a submerged shock-wave sensor, a hydrophone, and a PVDF sensor were used. As the cavitation impact energy can be obtained using an AE sensor and/or a laser Doppler vibrometer [41], these can be useful for measuring and/or monitoring the peening intensity of laser cavitation peening. During submerged laser peening, peening with and without a sacrificial overlay can be carried out. In both cases, as a number of small particles are produced during the laser ablation, feeding with water is required to remove contamination. We discuss water quality later in this paper. Thus, the fundamental harmonic, i.e., a wavelength of 1064 nm, was used to generate laser cavitation during the additional experiment.

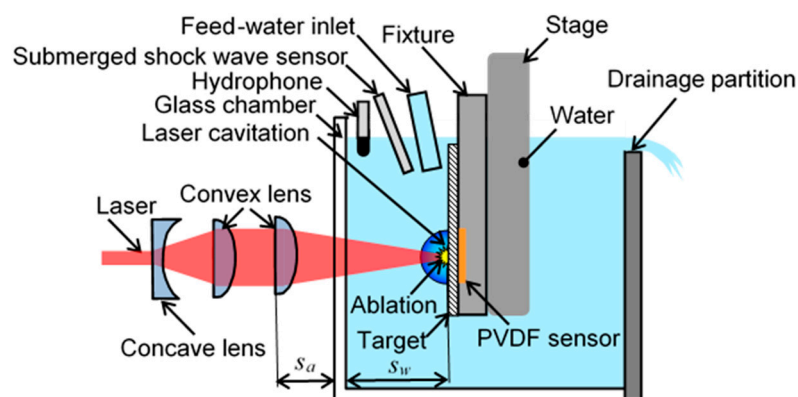


**Figure 5.** Schematic diagram of test section of laser cavitation peening system.

## 3. Comparison between Laser Ablation and Laser Cavitation

As it has been hypothesized that the laser ablation impact is used for submerged laser peening, we compared the pressures and/or impacts produced by laser ablation and laser cavitation collapse. Figure 6 shows (a) images of laser ablation, (b) the signal from the target from a PVDF sensor placed in the target, and (c) the signal from a shock-wave sensor in water [20]. At  $t = 0$  ms, both the PVDF sensor in the target and the submerged shock-wave sensor detected a pulse-like amplitude increase,

which was caused by the laser ablation. After laser ablation, a bubble was initiated and developed, then shrunk as in Figure 4 (a). When the bubble collapsed at  $t \approx 1$  ms, both the PVDF sensor and the submerged shock-wave sensor detected another pulse-like amplitude increase. When the amplitudes induced by the laser ablation and the laser cavitation collapse were compared, the amplitude of the laser cavitation collapse, measured using the PVDF sensor, was larger than that of the laser ablation. However, the amplitude detected by the submerged shock-wave sensor in respect of laser cavitation collapse was smaller than that of the laser ablation, as same as previous report [18]. The secondary collapse of the bubble at  $t \approx 1.5$  ms was detected by the PVDF sensor, but it was not detected by the submerged shock-wave sensor. It was suggested that the PVDF sensor could evaluate the impact more accurately than the submerged shock-wave sensor. When glycerol was used for the plasma confinement layer, the amplitude of the signal from a PVDF sensor during laser ablation was nearly equivalent to that of the laser cavitation collapse (see Figure 7).

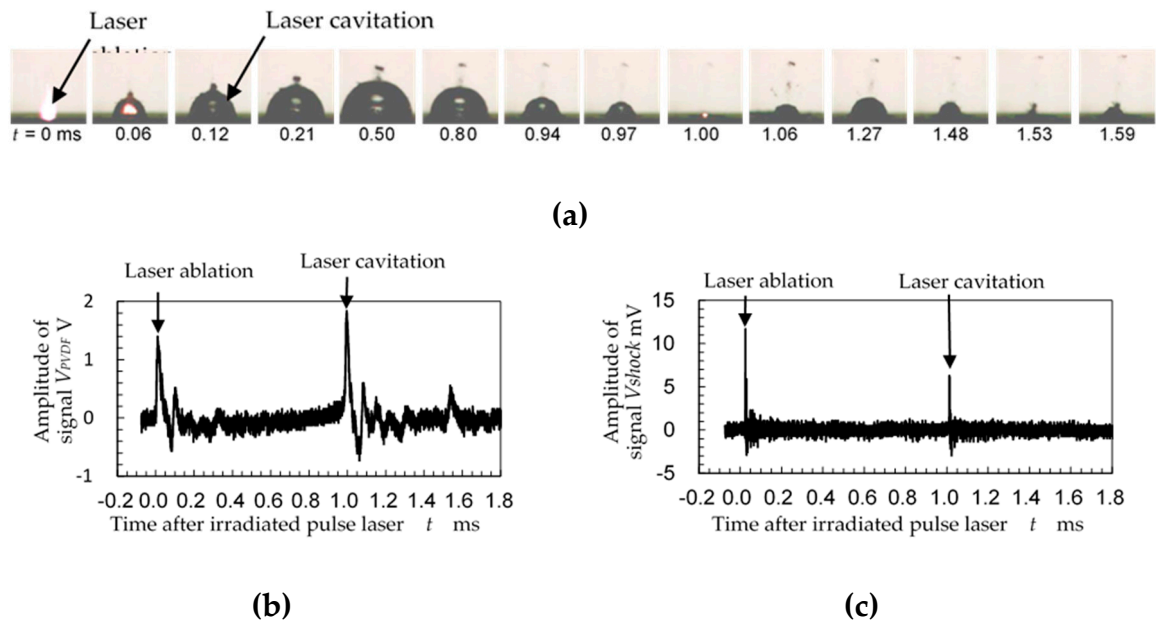


**Figure 6.** Laser ablation and laser cavitation produced by a pulsed laser: (a) images showing the development of laser ablation and laser cavitation; (b) signal from a PVDF sensor in the target; (c) signal from a shock-wave sensor in water. Reprinted from [20] with permission from Elsevier, License Number 5532490964237. .

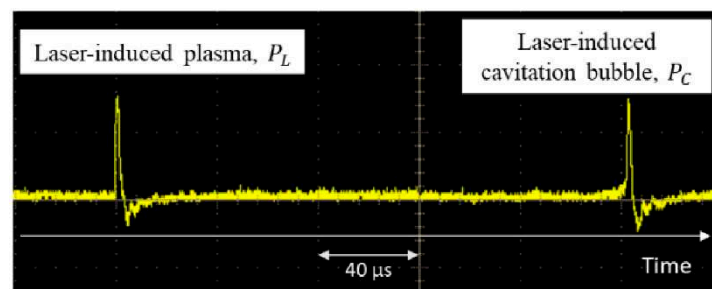


**Figure 7.** Shock-wave signal from laser-induced plasma and the collapse of the laser-induced cavitation bubble from a PVDF gauge sensor in glycerol. Reprinted from [42] with permission from Japan Laser Processing Society.

As a cavitation bubble collapse can be controlled by boundary conditions around the bubble, in one study, a pipe was placed near a target plate around the focus point and the arc-height of the target plate was measured [43]. The arc-height has been used for measurement of the peening intensity [44,45]. The inverse of curvature can be measured from the arc-height, and it is proportional

to the arc-height [46]. In Figure 8 (a), the target plate without a pipe was peened using submerged laser peening. Namely, both the laser ablation impact and laser cavitation collapse were used in Figure 8 (a), i.e., without a pipe in Figure 8 (c). However, a pipe was placed near the target plate around the focus point and peened in Figure 8 (b). As shown in the schematic above Figure 8 (b), when the pipe was placed near the wall, the bubble moved upwards and collapsed in the water rather than on the target surface. Thus, the peening intensity, i.e., the inverse of the curvature with the pipe, was nearly half of that without the pipe, as only the laser ablation impact was used; the laser cavitation collapse impact was not used during the peening with the pipe. It can be concluded that both the laser ablation impact and laser cavitation collapse impact are used during conventional submerged laser peening. Namely, one pulsed laser hits the surface twice. Regarding another important paper [47], during optimized laser cavitation peening, the laser cavitation collapse impact energy was 2.2 times larger than that of laser ablation.

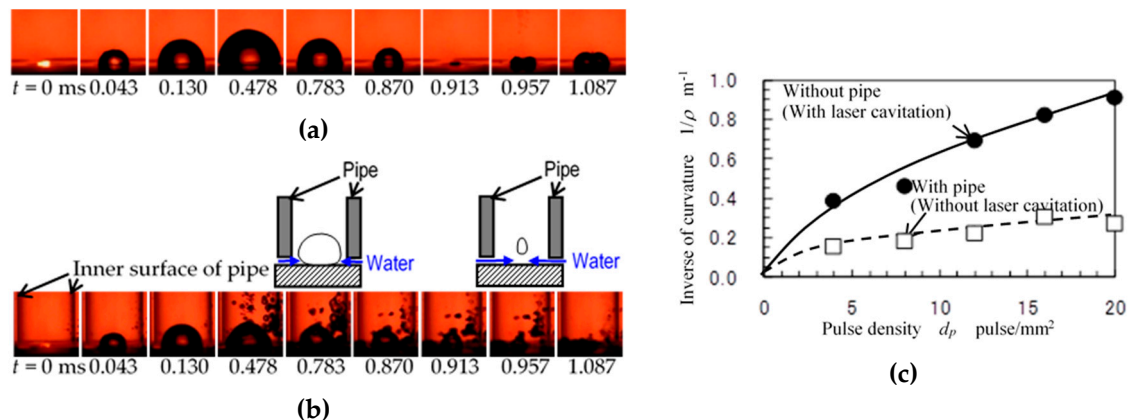


**Figure 8.** Effect of impact induced by laser cavitation on submerged laser peening: (a) images of laser cavitation without pipe; (b) images of laser cavitation with pipe; (c) effect of laser cavitation impact on peening intensity of submerged laser peening. Reprinted from [43] with permission from Japan Society of Shot Peening Technology.

## 4. Key Factors of Laser Cavitation Peening

### 4.1. Overview of Key Factors of Laser Cavitation Peening

Figure 9 reveals an overview of the mechanisms and key factors of laser cavitation peening. When a laser pulse with a pulse-width of several nanoseconds is irradiated to a target, laser ablation is generated, and laser ablation produces a shock-wave; then, the shock-wave initiates a bubble, i.e., laser cavitation. A laser pulse with a pulse-width of several hundred microseconds also generates laser cavitation due to sub-cool boiling [48,49]. In terms of the phase-change phenomenon from the liquid-phase to the gas-phase, this is affected by the characteristics of the liquid. The effect of the liquid was investigated in a previous study using pure water, glycerol, liquid paraffin, and silicone oil, and it was reported that the highest stress was observed in water [50]. The shock-wave and the microjet of the laser cavitation produce the impacts, as well as the shock-wave induced by the laser ablation. These impacts produce local plastic deformation pits on metallic materials. The local plastic deformation pits change the material properties, such as the residual stress, hardness, yield stress, tensile strength, dislocation density, grain size, Young's modulus, roughness, fracture toughness, etc. The compressive residual stress and the work-hardening introduced by laser cavitation peening can improve the fatigue strength and fatigue life. It has been reported that laser cavitation peening reduces crack initiation and crack propagation [51].

To generate a laser pulse, several laser systems are available. The main parameters of laser systems are the pulse width, pulse energy, wavelength, repetition frequency, beam diameter, etc. In a conventional laser cavitation peening system, the pulse width is several ns, the pulse energy is several hundred mJ, the wavelength is 532 nm or 1064 nm [16,20], repetition frequency is 10–200 Hz



[40], and the beam diameter is about a few mm. The effects of the pulse energy and the wavelength were discussed in a previous paper [16].

In the present review, the main factors related to laser cavitation collapse impact, such as bubble size, bubble shape, and water quality, are summarized. The effect of peening patterns is also discussed.

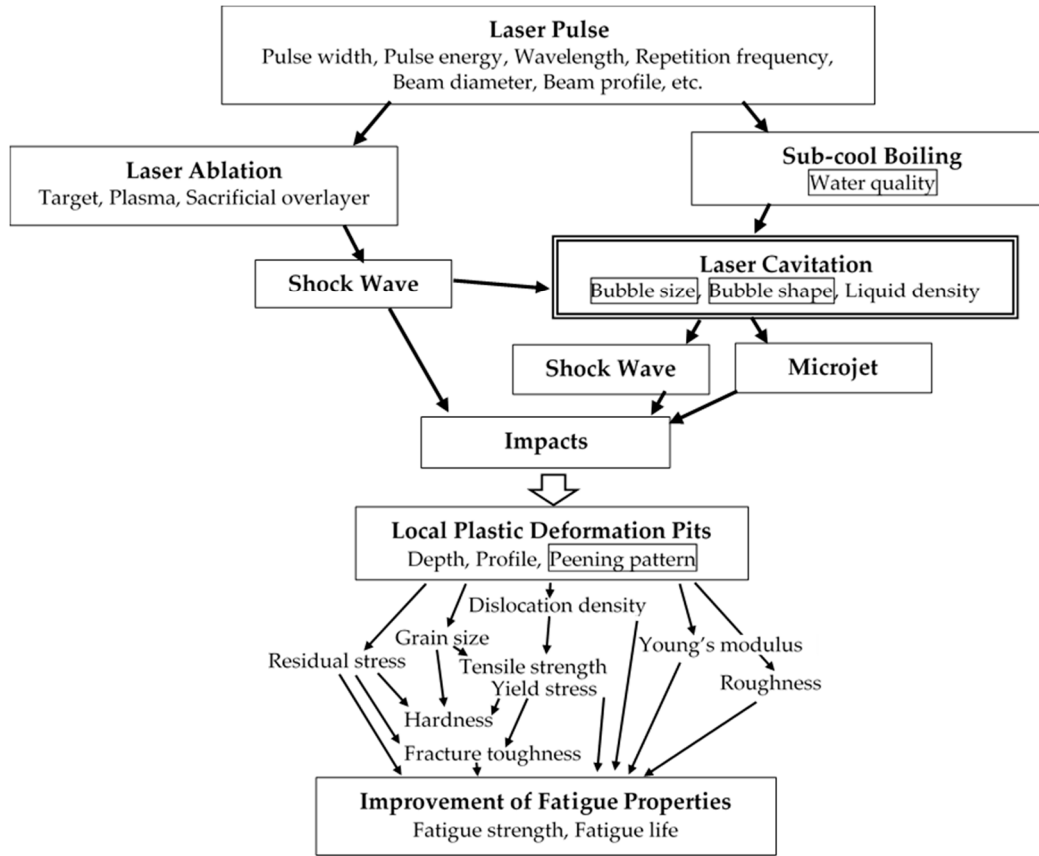


**Figure 9.** Schematic diagram of mechanisms and main factors of improvements in fatigue strength via laser cavitation peening.

#### 4.2. Bubble Size

As a larger bubble produces a larger impact during cavitation bubble collapse [52–55], the most important factor of laser cavitation peening is the bubble size. In order to demonstrate the monitoring of bubble size, Figure 10 shows the relationship between the developing time  $t_D$  and the diameter of laser cavitation  $d_{max}$  [16]. In Figure 10, the red circles show the data in respect of the hemispherical bubble and the other circles indicate the spherical bubble.  $t_D$  is defined as the time from laser ablation to the 1st collapse of the laser cavitation. For example, this was approximately 1 ms in the case of Figure 6. The  $d_{max}$  was evaluated using a high-speed video camera (see Figure 6 (a)). Figure 10 was obtained by changing the laser pulse energy. As shown in Figure 10,  $d_{max}$  [mm] is proportional to  $t_D$  [ $\mu$ s] and the relation is described as in Equation (1), including both spherical and hemispherical bubbles.

$$d_{max}[\text{mm}] = 0.0103 t_D [\mu\text{s}] \quad (1)$$

Regarding Rayleigh [56], the collapse time for a bubble of diameter  $R_0$  is given by Equation (2).

$$t_c = 0.91468 R_0 \sqrt{\frac{\rho}{p}} \quad (2)$$

When the values  $p = 0.1013$  MPa and  $\rho = 998$  kg/m<sup>3</sup> are substituted into Equation (2), Equation (3) is obtained.

$$R_0 [\text{mm}] = 0.0111 t_c [\mu\text{s}] \quad (3)$$

By definition,  $R_0$  is half of  $d_{\max}$  and  $t_c$  is half of  $t_D$ , so the proportional constants in Eqs. (1) and (3) are almost equivalent. Thus, it was concluded that the bubble size can be evaluated by measuring the developing time of the bubble.

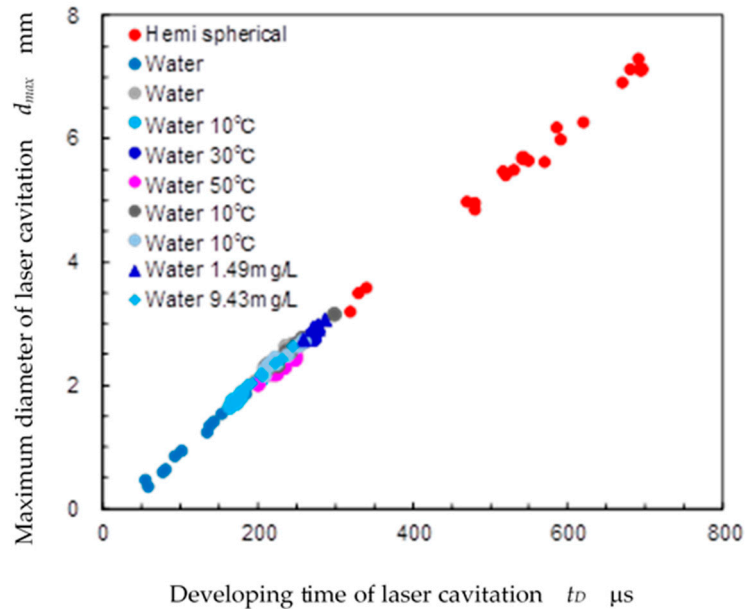


**Figure 10.** Relation between developing time and diameter of bubble [16].

In order to reveal the relation between bubble size and peening intensity, Figure 11 shows the relation between the developing time  $t_D$  and the arc-height  $h$  [16]. As shown in Equation (1), the bubble size can be estimated using  $t_D$ . As mentioned in the explanation of Figure 8, the peening intensity can be evaluated using the arc-height. In Figure 11, duralumin, stainless steel, and N-strip were used; duralumin was a soft metal and N-strip was a hard material compared with stainless steel. Thus, the threshold impact, which corresponds to the material hardness, was assumed. When the threshold impact was assumed, the arc-height was proportional to the maximum volume of the laser cavitation [16]. This would be reasonable, as the cavitation intensity is proportional to the volume [52–55].

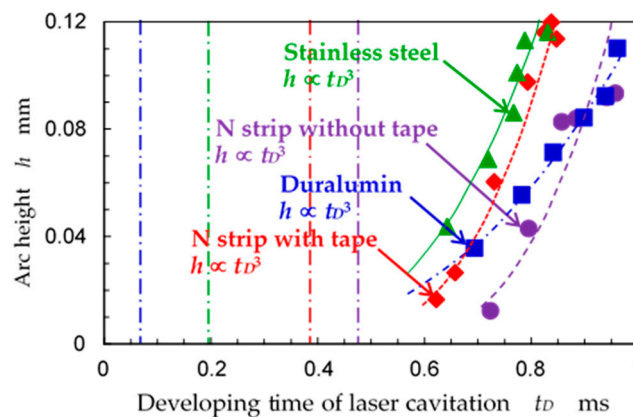


**Figure 11.** Effect of laser cavitation volume on peening intensity [16].

#### 4.3. Bubble Shape

In this section, we investigate the effect of bubble shape. Figure 12 shows images of laser cavitation. In Figure 12, the specimen was set closer than the optimal  $s_w$  in Figure 5. When  $s_w$  was large enough, the laser cavitation developed as a hemispherical bubble, as shown in Figure 6 (a). However, when  $s_w$  was shorter than the optimal  $s_w$ , the bubble developed into a flattened hemispherical bubble, i.e., a pancake-shaped bubble, i.e.,  $t = 0.04 - 0.22$  ms, as shown in Figure 12. During the shrinking of the bubble, it became a longitudinal bubble, as shown at  $t = 0.70$  ms, then collapsed.

Figure 13 shows the bubble that developed at the edge. When the pulsed laser was irradiated at the edge, the bubble developed at the edge, and the outer shape was nearly a spherical bubble, i.e.,  $t = 0.09 - 0.43$  ms, as shown in Figure 13. During the shrinking of the bubble, it became a kind of horn-shape, then collapsed. After the first collapse, the other two bubbles were generated and then collapsed. One of the secondary bubbles became considerably large, and then collapsed. In order to illustrate the effect of the bubble that developed at the corner, Figure 14 shows the distribution of surface residual stress measured using a collimator of 0.146 mm in diameter via the 2D method [57]. The target material of Figure 14 was titanium alloy Ti6Al4V. After laser cavitation peening at 30 and 40 pulse/mm<sup>2</sup>, compressive residual stress of about 100 MPa was introduced, and the compressive residual stress introduced near the corner was almost equivalent to the value at the center of the specimen. Namely, a bubble developed at the corner can introduce compressive residual stress into titanium alloy Ti6Al4V.

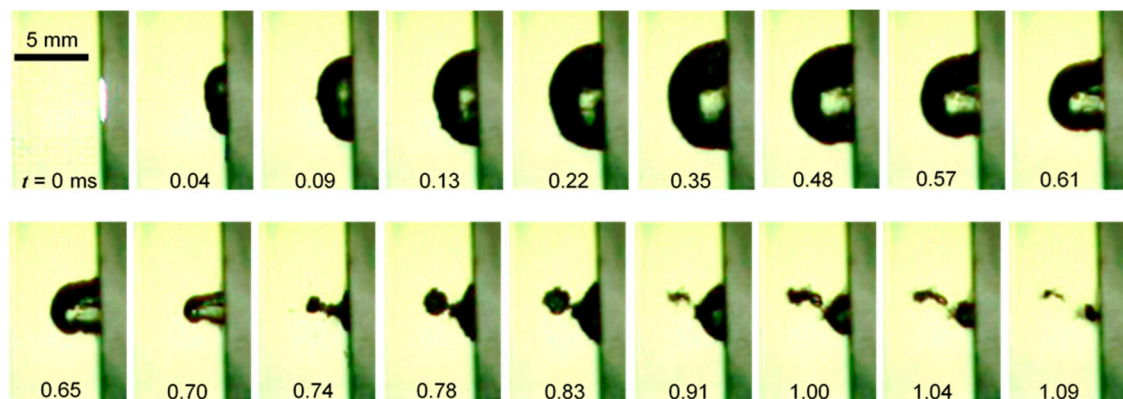


**Figure 12.** Images of laser cavitation on the wall near the glass chamber.

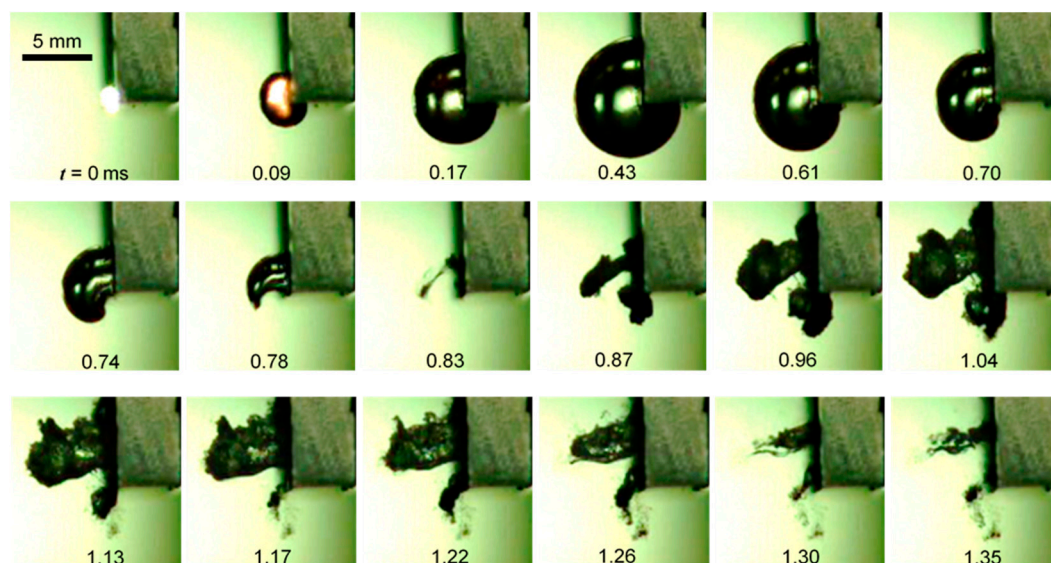


**Figure 13.** Images of laser cavitation on the wall near the edge.

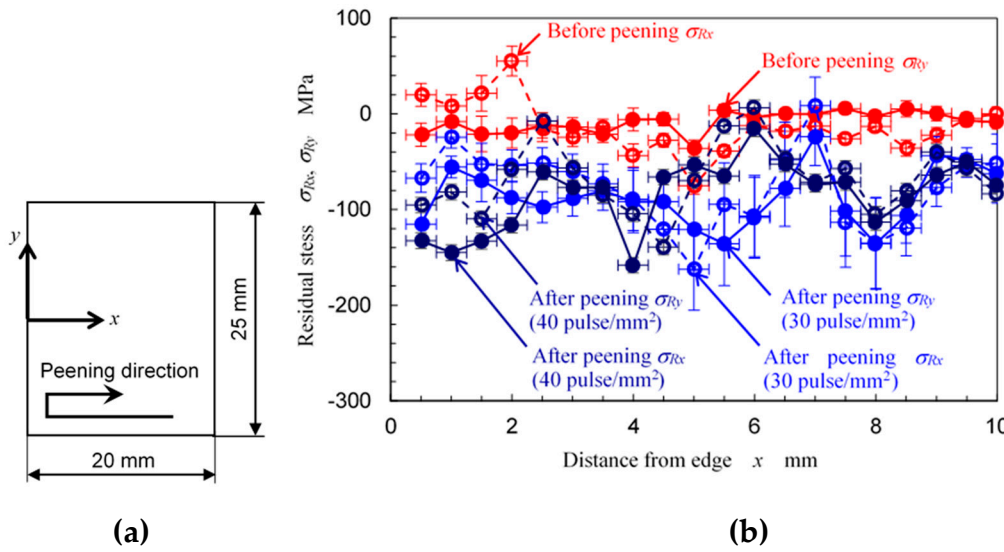


**Figure 14.** Introduction of compressive residual stress via laser cavitation peening to surface near edge of titanium alloy Ti6Al4V: (a) peening direction and definition of residual stress; (b) residual stress changing with distance from edge before and after peening.

Next, we compare experimentally microjet-type bubbles, as shown in Figure 2 (a), and hemispherical bubbles, as shown in Figure 2 (b). Figure 15 shows the behavior of a bubble, which was developed near the target surface by focusing in water [58]. The bubble was initiated in water near the target and developed, then collapsed in water. After that, the bubble was developed on the target, then collapsed on the target.

In order to compare the peening intensity of the bubble shown in Figure 15 and the hemispherical bubble, Figure 16 illustrates the residual stress as a function of the distance from the target surface. The blue line shows the residual stress of stainless steel treated at 10 pulse/mm<sup>2</sup> by the bubble shown in Figure 15 [59], and the violet line shows treatment at 4 pulse/mm<sup>2</sup> by the hemispherical bubble [6]. The red line reveals the residual stress without peening [59]. For both treatments, a Q-switched Nd:YAG laser of 0.35 J and 1064 nm was used. As shown in Figure 16, the hemispherical bubble at 4 pulse/mm<sup>2</sup> introduced large compressive residual stress into a deeper region compared with the bubble shown in Figure 15 at 10 pulse/mm<sup>2</sup>. Namely, the collapse of the hemispherical bubble produced a more intense impact compared with the microjet.

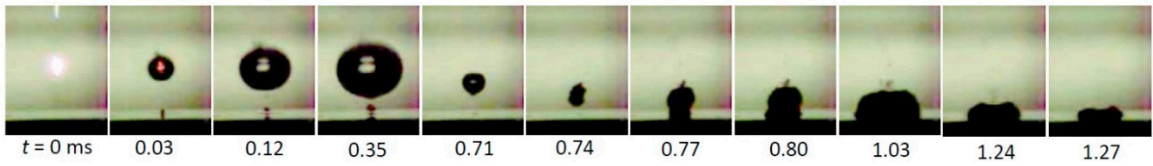
Now, we investigate the effect of the bubble shape using numerical simulation. Iga and Sasaki carried out a fluid/material-coupled numerical simulation of the first stage of the non-spherical collapse of a bubble near a wall, including the stress state inside the elastic material of the wall [35]. Figure 17 shows the results of typical cases (a)  $\gamma = -0.3$ , (b)  $\gamma = 0$ , and (c)  $\gamma = 1.2$  [35]. In Figure 17,  $\gamma$  is defined by the distance between the center of the bubble and the wall surface,  $L$ , and the maximum bubble radius is  $R_{max}$ , as per Equation (4).

$$\gamma = \frac{L}{R_{max}} \quad (4)$$

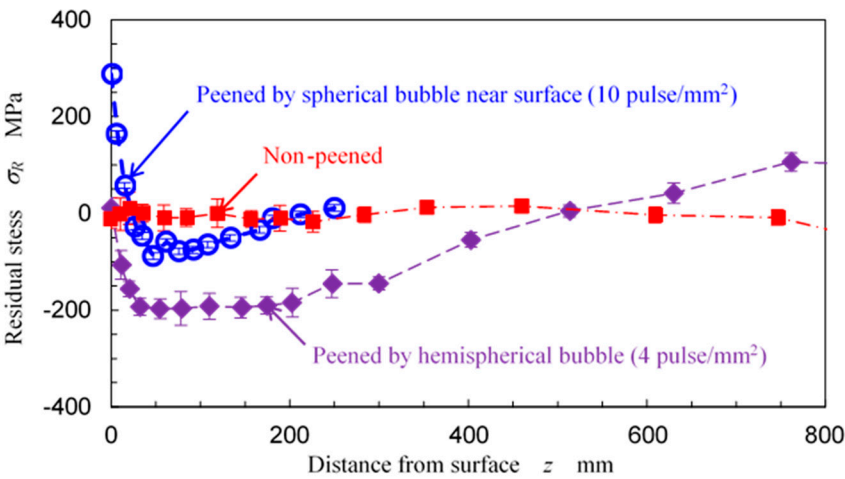
(a)  $\gamma = -0.3$  corresponds to a pancake-shaped bubble, as shown in Figure 12, (b)  $\gamma = 0$  corresponds to a hemispherical bubble, as shown in Figure 6 (a), and (c)  $\gamma = 1.2$  shows the bubble near the wall, as shown in Figure 15. In the case of (c)  $\gamma = 1.2$ , the bubble has collapsed, generating a microjet. Iga and Sasaki simulated the void fraction, pressure in water, and equivalent stress of the material at various values of  $\gamma$  [35]. Three color bars for each value are shown in the upper part of Figure 17. Figure 17 reveals contours of the values changing with the time. As shown in Figure 17 (a)  $\gamma = -0.3$ , i.e., the pancake-shaped bubble, part of bubble near the wall shrunk quicker than the top of the bubble; it became a longitudinal bubble at  $t = 83.8 \mu s$ . The longitudinal shape was very similar to the



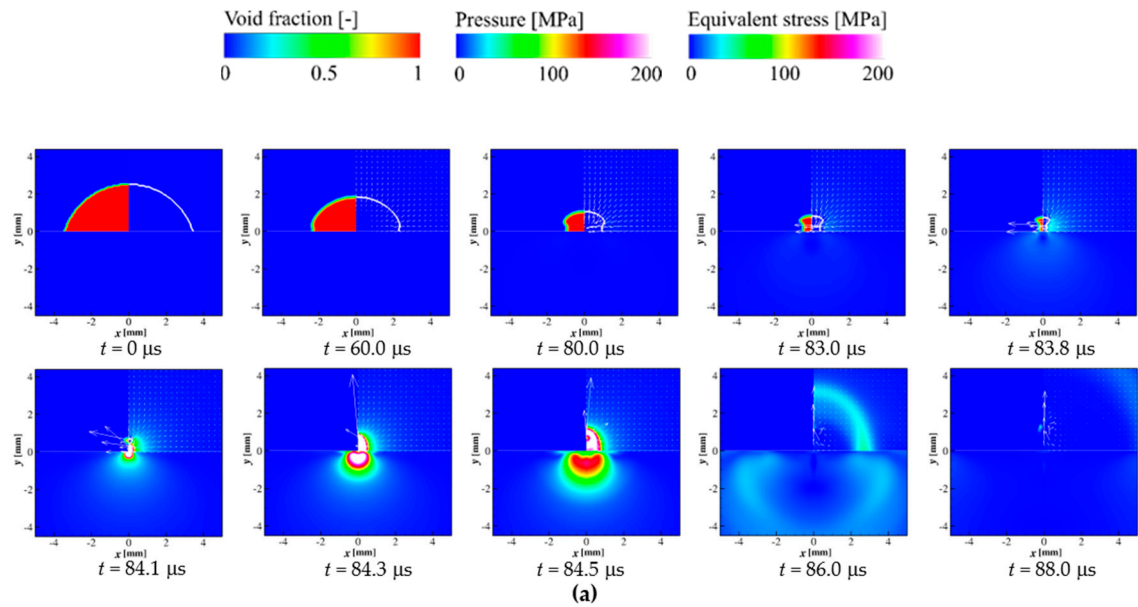
longitudinal bubble at  $t = 0.70$  ms in Figure 12.  $t = 0$  ms in Figure 12 corresponds to the irradiation of the pulsed laser.



**Figure 15.** Images of laser cavitation focused in the water by pulsed laser near the wall [58].



**Figure 16.** Distribution of residual stress of stainless steel introduced by laser cavitation peening [6,59].





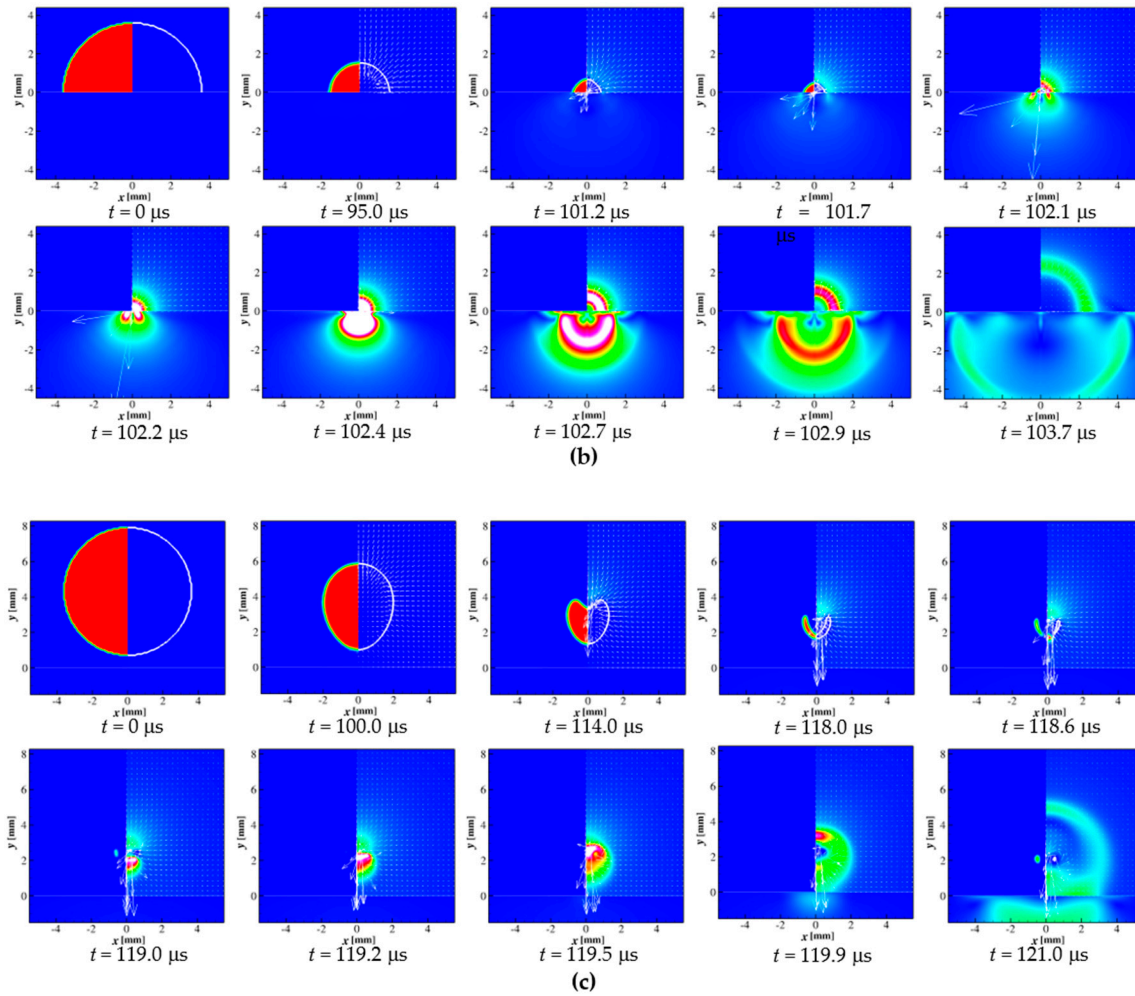


**Figure 17.** Fluid/material-coupled numerical simulation of collapse of a bubble: (a) pancake-shaped bubble on the wall ( $\gamma=-0.3$ ); (b) hemispherical bubble on the wall (hemispherical mode;  $\gamma=0$ ); (c) spherical bubble near the wall (microjet mode;  $\gamma=1.2$ ) [35].

However,  $t = 0 \mu\text{s}$  in Figure 17 is the time at which the radius of the bubble reached a maximum. As shown in Figs. 12 and 17 (a), the fluid/material-coupled numerical simulation revealed experimental results. In the case of the hemispherical bubble collapse shown in Figure 17 (b), the pressure around the bubble became larger than that inside the bubble. This is similar to the phenomenon reported after theoretical analysis [60]. As shown in Figure 17 (c), a microjet is generated, and this causes a water-hammer effect.

In order to consider the effect of bubble shape on peening and/or erosion via cavitation bubble collapse, Figure 18 shows variations in the maximum equivalent stress and stress influence area changing with  $\gamma$ . The maximum equivalent stress had a maximum at  $\gamma = 0$ . Namely, the impact caused by the hemispherical bubble,  $\gamma = 0$ , was larger than that of the microjet-mode bubble  $\gamma = 1.2$ . Further, the stress influential volume has a maximum at  $\gamma = 0$ . Namely, the hemispherical bubble collapse affects the wider volume compared with microjet-type collapse, as shown in Figure 18 (b). Note that the collapse of the bubble at  $\gamma = 0.5$  affects a deeper region compared with the bubble at  $\gamma = 0$ . Considering the results of Figure 18 (a)-(c), the collapse of the hemispherical bubble at  $\gamma = 0$  is suitable for laser cavitation peening.

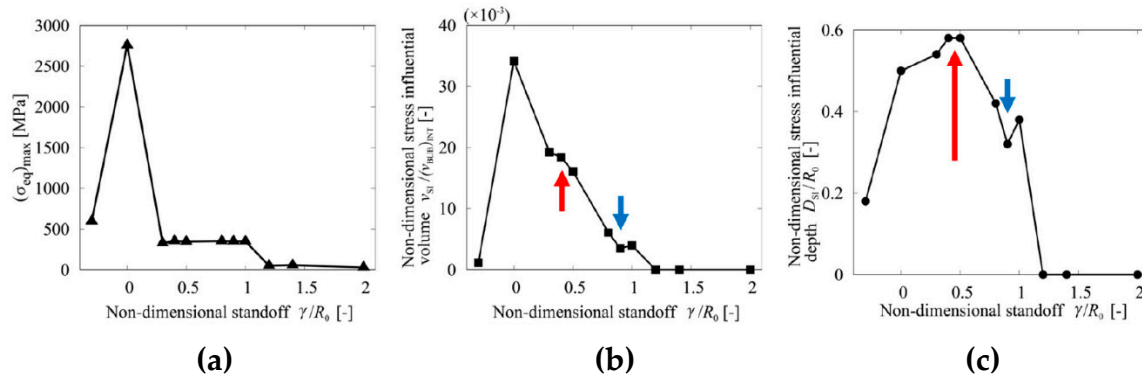


**Figure 18.** Variations in maximum equivalent stress and stress influence area with the stand-off distance between the bubble and the wall; (a) maximum equivalent stress; (b) volume of stress influence area; (c) depth of stress influence area [35].

#### 4.4. Water Quality

In order to investigate the effect of feeding water on peening intensity, Figure 19 shows the arc-height changing with the laser pulse density at various conditions using an aluminum plate. During the present condition, the flow rate of the feeding water was 5 L/min. The oxygen content was 6.4 mg/L without degassing and 1.6 mg/L with degassing. The water temperature was about 283 K. As shown in Figure 19, the arc-height of laser cavitation peening with feeding water was larger than that of the peening without feeding water, as the feeding water removed small particles that were caused by laser ablation. The small particles might obstruct the laser from reaching the target surface. If the air content in the water was large, the minimum size of the cavitation bubble was larger. Thus, the rebound after the cavitation bubble collapse was slightly slower, and the impact during bubble collapse was reduced. This is called the “cushion effect”. Namely, the cavitation bubble collapse impact is affected by the air content of the water. As shown in Figure 19, the arc-height of laser cavitation peening with degassed feeding water was larger than that of non-degassed feeding water. Thus, in order to minimize the cushion effect, feeding with degassed water is suitable for laser cavitation peening.

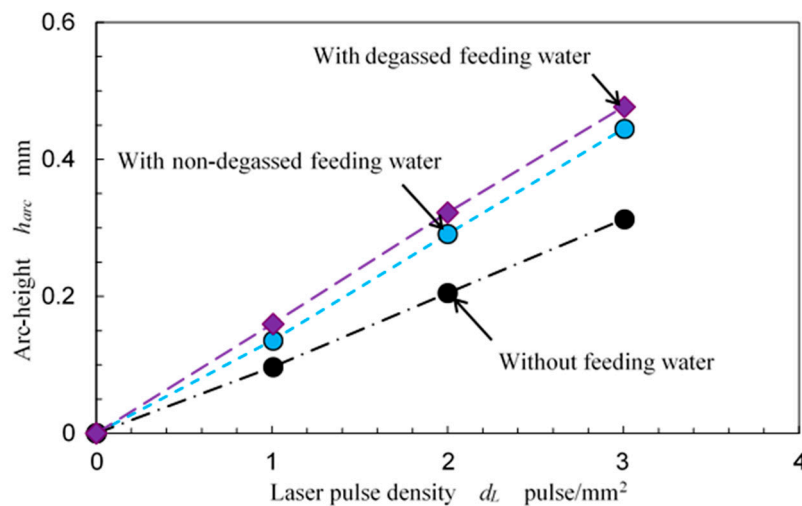


**Figure 19.** Effect of feeding water on peening intensity measured using arc-height of aluminum plate.

#### 4.5. Peening Pattern

In order to reveal the effect of the peening pattern, Figure 20 shows the surface residual stress changing with the irradiation step in the  $x$ - and  $y$ -directions, as shown in the upper part of Figure 20.

For all three cases, similar compressive residual stress was introduced, even though anisotropic irradiation was applied. Note that the virgin surface was treated.

In order to investigate the effects of overstrike during laser cavitation peening, Figure 21 reveals the fatigue life of titanium alloy Ti6Al4V manufactured via direct metal laser sintering. The fatigue life was evaluated using a torsion fatigue tester [60]. For all five cases, the total laser pulse density was 40 pulse/mm<sup>2</sup>. In the case of 40 pulse/mm<sup>2</sup>, both the step distance in the circumferential direction and axial direction was 0.158 mm. In the case of 5 + 35 pulse/mm<sup>2</sup>, the step distances in both the circumferential and axial directions were 0.447 mm at the 1st step and 0.169 mm at the 2nd step. For all five cases, the fatigue life was improved compared with as-built specimen. The first 5 pulse/mm<sup>2</sup> and the second 35 pulse/mm<sup>2</sup> had the longest life. When Ti6Al4V was treated via laser cavitation peening, the surface was oxidized. It was reported that the oxidized layer of Ti6Al4V after laser cavitation peening was Ti<sub>4</sub>O<sub>5</sub> [10]. As the color of Ti<sub>4</sub>O<sub>5</sub> is black, the irradiated laser energy was more intense compared with treatment of the virgin surface, which is blighter than Ti<sub>4</sub>O<sub>5</sub>. As the local surface residual stress changed in between laser spots [57], the higher the laser density at the last stage of laser cavitation peening, the longer the fatigue life.

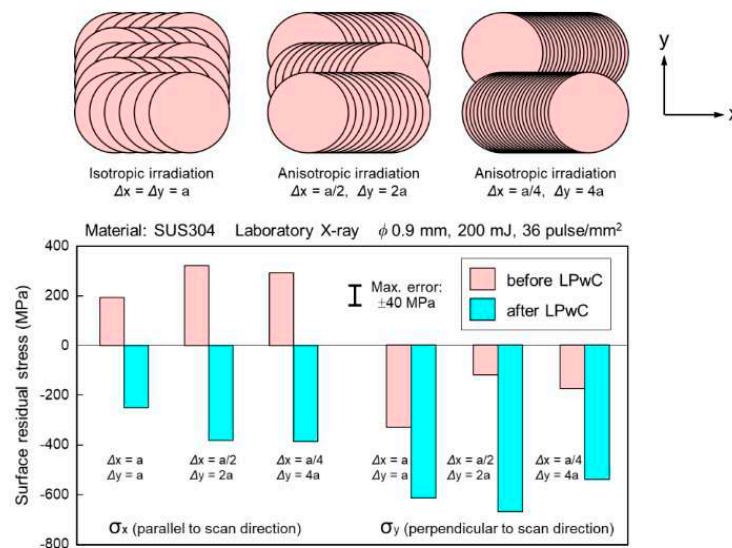


**Figure 20.** Surface residual stresses before and after area isotropic and anisotropic irradiation [15].

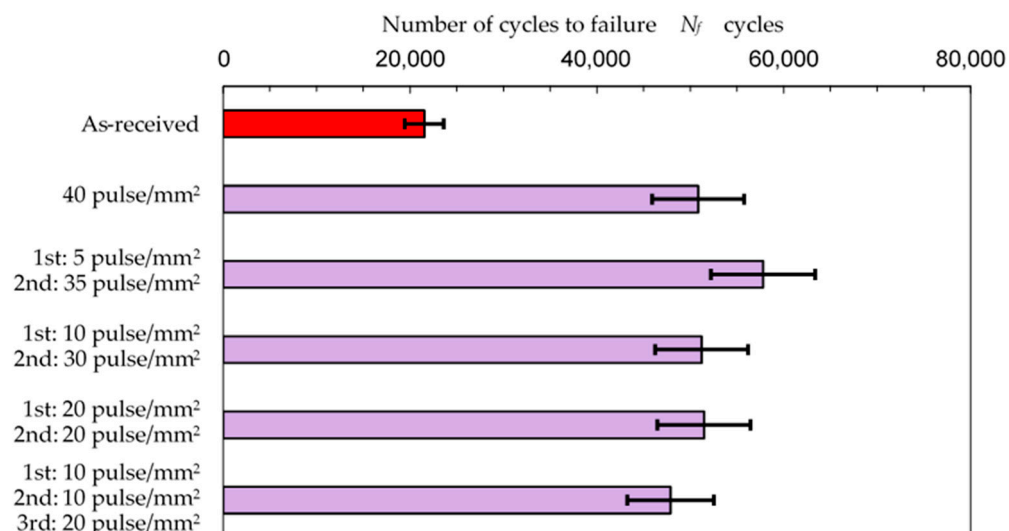


**Figure 21.** Effect of peening pattern on improvement of fatigue life at  $\tau_a = 460$  MPa for additive manufactured titanium alloy Ti6Al4V via direct metal laser sintering.

## 5. Improvement of Fatigue Properties of Metals via Laser Cavitation Peening

In order to reveal the improvement of the fatigue properties of 3D metals via laser cavitation peening, Figure 22 shows the  $S-N$  curves of additive-manufactured titanium alloy Ti6Al4V via direct metal laser sintering (DMLS) treated using laser cavitation peening, compared with a non-peened (as-built) specimen [60]. As shown in Figure 22, the fatigue life was improved by laser cavitation peening (CP by laser).

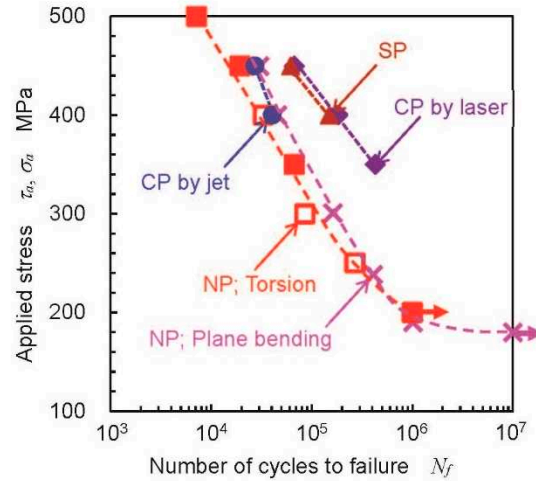


**Figure 22.** Improvement of fatigue life of titanium alloy Ti6Al4V additively manufactured via direct metal laser sintering using laser cavitation peening (CP by laser), compared with shot peening and cavitation peening using a jet. Reprinted from [60] with permission from Elsevier, License Number 5532491421394.

Figure 23 shows images of additive manufactured titanium alloy Ti6Al4V produced using DMLS: (a) as-built specimen and (b) laser cavitation peened specimen [10]. Many unmelted particles were observed on the surface of the as-built specimen, and the maximum height of roughness  $R_z$  was about 140  $\mu\text{m}$ . After laser cavitation peening,  $R_z$  decreased to about 100  $\mu\text{m}$ , and compressive residual stress was introduced [10]. The hardness was also increased. Thus, the reduction in surface roughness and the introduction of compressive residual stress and work-hardening are the reasons why laser cavitation peening improves the fatigue properties of 3D metals.

Table 1 shows the fatigue strength at  $10^7$  of non-peened metallic materials and materials that underwent laser cavitation peening compared with shot peening. The fatigue strength at  $10^7$  was calculated using Little's method [61]. Figure 24 illustrates the relationship between the fatigue strength of the non-peened specimen  $\sigma_{fN}$ ,  $\tau_{fN}$  and the fatigue strength of the peened specimen  $\sigma_{fP}$ ,  $\tau_{fP}$ . As shown in Table 1 and Figure 24, both laser cavitation peening and shot peening improve the fatigue strength compared with the non-peened specimen. When the proportional constant is considered, laser cavitation peening and shot peening can be described as in Eqs. (5) and (6).

$$\sigma_{fP}, \tau_{fP} = 1.52 \pm 0.15 \sigma_{fN}, \tau_{fN} \quad (5)$$

$$\sigma_{fP}, \tau_{fP} = 1.41 \pm 0.15 \sigma_{fN}, \tau_{fN} \quad (6)$$

Namely, laser cavitation peening can improve fatigue strength by 10% over shot peening. In order to consider the difference in the improvement of fatigue strength between laser cavitation peening and shot peening, Figure 25 reveals an EBSD analysis of the cross-section after a) cavitation peening CP using a cavitating jet, b) shot peening SP, and c) cavitation peening using a laser, i.e., laser cavitation peening [62]. During the experiment, stainless steel plate was treated so that the arc-height was equivalent in all three cases. As shown in Figure 25, the dislocation density of cavitation peening using both jet and laser was less than that of shot peening. As the dislocations might become a source of crack initiation, the fatigue properties of shot peening would be weaker than that of

cavitation peening. As is known, the compressive residual stress introduced by the surface treatments was released, and the relaxation of the compressive residual stress depended on the treatment methods [66–70]. It was reported that the relaxation of compressive residual stress introduced by cavitation peening is less than that of shot peening [71]. This would be another reason why the fatigue performance of cavitation peening is better than that of shot peening.

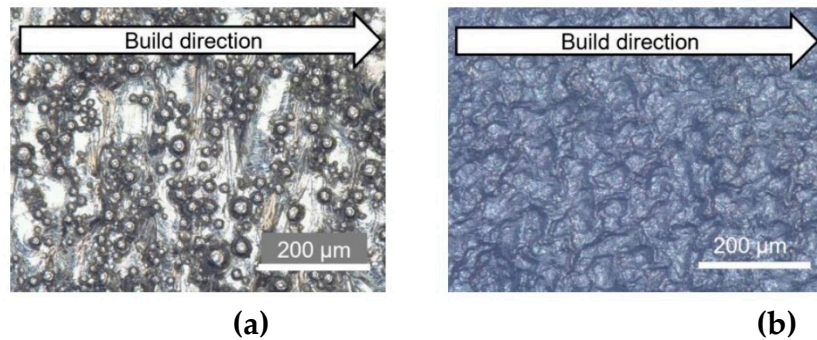


**Figure 23.** Images of surface of additive-manufactured titanium alloy Ti6Al4V via direct metal laser sintering: (a) as-built; (b) laser cavitation peening [10].

**Table 1.** Improvement in fatigue life of metallic materials via laser cavitation peening compared with non-peened and shot peening.

Material	Fatigue test	Fatigue strength at $10^7$			Reference
		Non-peened	Laser cavitation peening	Shot peening	
AM (EBM) titanium alloy Ti6Al4V	Plane bending	169 MPa	317 MPa	335 MPa	[7]
AM (DMLS) titanium alloy Ti6Al4V	Plane bending	185 MPa	357 MPa	355 MPa	[63]
AM (DMLS) titanium alloy Ti6Al4V	Torsion	217 MPa	361 MPa	285 MPa	[64]
Magnesium alloy AZ31B	Plane bending	97 MPa	151 MPa	104 MPa	[65]
Stainless-steel 316L	Plane bending	279 MPa	272 MPa	305 MPa	[20]
Stainless-steel 316L (welded)	Plane bending	188 MPa	300 MPa	260 MPa	[16]

AM: Additive manufacturing; EBM: Electron beam melting; DMLS: Direct metal laser sintering.

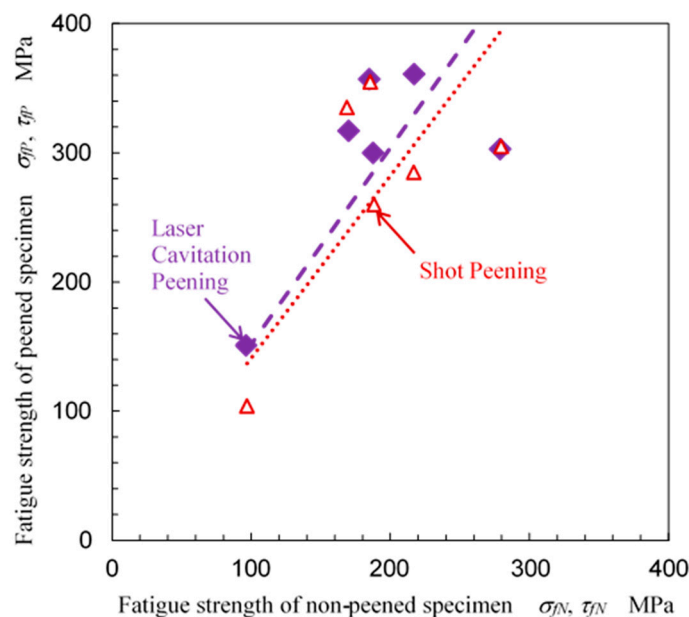


**Figure 24.** Improvement in fatigue strength of metallic materials via laser cavitation peening compared with shot peening.



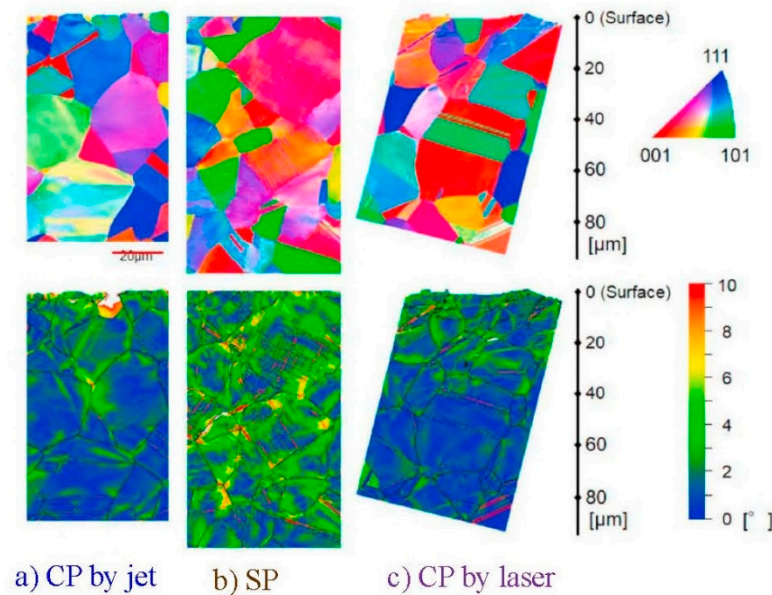


**Figure 25.** EBSD analysis of cross-section after a) CP via jet, b) SP, and c) CP via laser (laser cavitation peening) surface treatments showing inverse pole figure maps (top) relative to the normal to the cross-section, and grain reference orientation deviation (GROD) maps (bottom). Reprinted from [62] with permission from Elsevier, License Number 5532500298391.

## 6. Future Work

One of major issues in laser cavitation peening is the drastic improvement in efficiency, as it takes time to enhance the fatigue properties of metallic materials. During conventional laser cavitation peening, a Nd:YAG laser with a Q-switch is used, as the impact induced by laser ablation is also utilized. As mentioned in this review paper, when suitable conditions such as the feeding of degassed water to enhance the laser cavitation collapse impact are applied, the laser cavitation impact can treat metallic materials. If the laser cavitation impact without the laser ablation impact can treat the metallic materials, a short laser pulse, whose pulse width is a few ns to generate laser ablation, is not required. It was reported that a Er:YAG laser, whose pulse width is 300  $\mu\text{s}$ , can produce laser cavitation [48]. When a laser pulse of several hundred  $\mu\text{s}$  in pulse width can be used for laser cavitation peening, the processing efficiency of laser cavitation peening can be drastically improved. Other types of laser system, such as fiber lasers, whose repetition frequency is 50 kHz, can be used for laser cavitation peening. Currently, the repetition frequency range of a conventional Nd:YAG laser with a Q-switch is dozens of Hz to hundreds of Hz. Thus, one of the future research directions in respect of laser cavitation peening is the research and development of laser cavitation peening using a pulse laser with a longer pulse width to increase the repetition frequency.

In order to reveal the possibility of laser cavitation peening using a long laser pulse, Figure 26 shows (a) images of laser cavitation and (b) the pressure detected by a hydrophone [72]. The pulse laser used was a Nd:YAG laser without a Q-switch, i.e. normal oscillation, whose pulse width was about 200  $\mu\text{s}$ . As a Q-switch was not used, the high-speed observation and the recording of the output signal from the hydrophone were not synchronized. As shown in Figure 26 (a), a relatively long laser pulse such as 200  $\mu\text{s}$  can generate a bubble, and the bubble developed and then collapsed in the same way as in Figure 7 (a). During laser ablation, i.e.,  $t = 0$  ms, a small pressure pulse was detected, as shown in Figure 26 (b). The large signal was observed during the 1st collapse of the laser cavitation. However, during the 2nd collapse of the laser cavitation, the amplitude of the signal was larger than that of the laser ablation. Namely, a relatively long laser pulse such as 200  $\mu\text{s}$  can generate laser cavitation and this can be applicable for laser cavitation peening. Thus, other types of laser, such as fiber lasers, can be utilized for laser cavitation peening to drastically increase efficiency. In order to optimize laser cavitation peening using a long laser pulse, the effect of parameters such as the laser

energy, repetition frequency, standoff distance, and focal distance of the lens should be investigated, as laser cavitation peening utilizes a sub-cooling phenomenon, as shown in Figure 9.

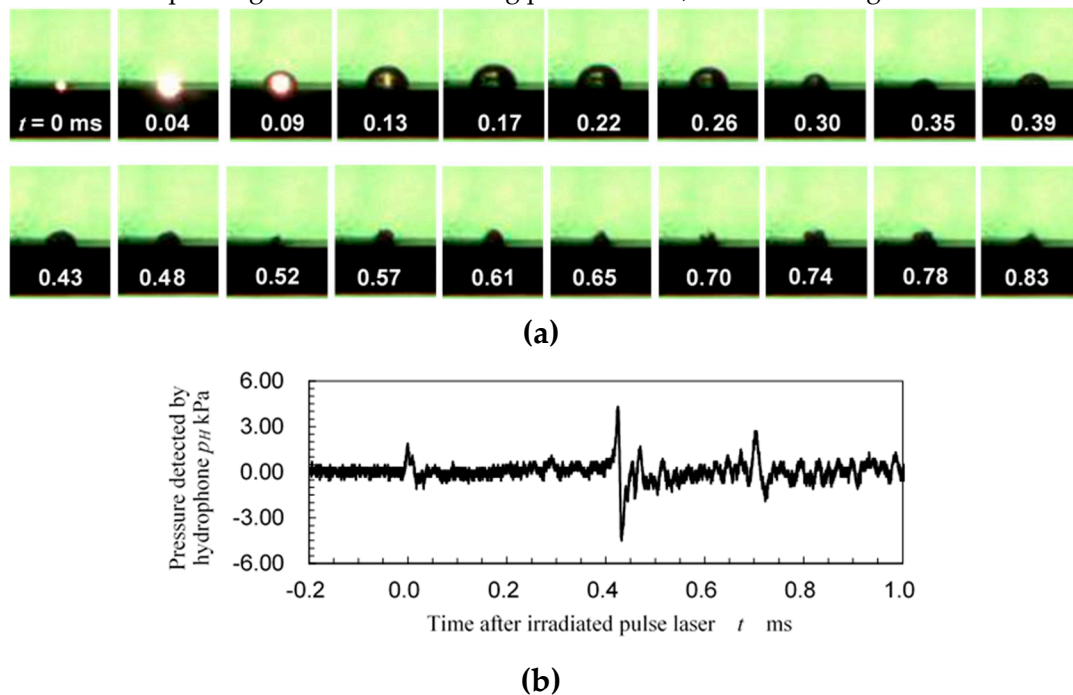


**Figure 26.** Laser cavitation generated by Nd:YAG laser without Q-switch: (a) images of laser ablation and laser cavitation; (b) Pressure detected by hydrophone [72].

## 7. Conclusions

In order to reveal the importance of the collapse impact of the bubble, which develops after laser ablation during submerged laser peening, the peening method was named “laser cavitation peening”, and the impact during bubble collapse was compared with the impact during laser ablation using published papers. The types of laser cavitation were reviewed by summarizing experimental data and numerical simulations, with additional observation of laser cavitation. To show the effect of laser cavitation peening on the improvement of the fatigue properties of metallic materials, including 3D metals, the fatigue life and strength of materials after laser cavitation peening were compared with non-peened samples. The findings of the present review can be summarized as follows:

- (1) During submerged laser peening, the impact of laser cavitation, which is generated after laser ablation, can be utilized for mechanical surface treatment. This is referred to as laser cavitation peening. Water quality, such as gas content, is an important factor, as the cavitation bubble collapse impact is affected by the gas content; this is called the cushion effect.
- (2) The impact passing through the target of laser cavitation collapse is greater than that of laser ablation, although the amplitude of the shock-wave in water induced by laser ablation is larger than that of laser cavitation collapse.
- (3) A hemispherical bubble is most effective for laser cavitation peening compared with a spherical bubble, which produces a microjet in the bubble.
- (4) In the case of laser cavitation peening, the peening intensity is proportional to the volume of laser cavitation when the threshold of the target materials is considered.
- (5) During laser cavitation peening, the area near the edge can be treated using laser cavitation, which develops and collapses near the edge.
- (6) Laser cavitation peening improves the fatigue strength of metallic materials, including three-dimensional additively manufactured metals (3D metals).

**Author Contributions:** Hitoshi Soyama: conceptualization, additional experiment, writing—original draft, visualization, project administration, funding acquisition. Yuka Iga: conceptualization, visualization, writing—review and editing.

**Funding:** This research was partly supported by JSPS KAKENHI grant numbers 23H01292 and 22KK0050, and the Amada Foundation AF-2021219-B3.

**Data Availability Statement:** The data presented in this study are available upon request from the authors.

**Conflicts of Interest:** The authors declare no conflicts of interest.

## References

1. Wagner, L. Mechanical surface treatments on titanium, aluminum and magnesium alloys. *Mater. Sci. Eng. A* **1999**, 263, 210-216.
2. Wang, P.; Li, X.; Luo, S.; Nai, M.L.S.; Ding, J.; Wei, J. Additively manufactured heterogeneously porous metallic bone with biostructural functions and bone-like mechanical properties. *J. Mater. Sci. Technol.* **2021**, 62, 173-179.
3. Edwards, P.; O'Conner, A.; Ramulu, M. Electron beam additive manufacturing of titanium components: Properties and performance. *J. Manuf. Sci. Eng.* **2013**, 135, 061016.
4. Peyre, P.; Fabbro, R.; Merrien, P.; Lieurade, H.P. Laser shock processing of aluminium alloys. Application to high cycle fatigue behaviour. *Mater. Sci. Eng. A* **1996**, 210, 102-113.
5. Sano, Y. Quarter century development of laser peening without coating. *Metals* **2020**, 10, 152.
6. Soyama, H.; Korsunsky, A.M. A critical comparative review of cavitation peening and other surface peening methods. *J. Mater. Process. Technol.* **2022**, 305, 117586.
7. Soyama, H.; Okura, Y. The use of various peening methods to improve the fatigue strength of titanium alloy Ti6Al4V manufactured by electron beam melting. *AIMS Mater. Sci.* **2018**, 5, 1000-1015.
8. Hackel, L.; Rankin, J.R.; Rubenchik, A.; King, W.E.; Matthews, M. Laser peening: A tool for additive manufacturing post-processing. *Addit. Manuf.* **2018**, 24, 67-75.
9. Kahlin, M.; Ansell, H.; Basu, D.; Kerwin, A.; Newton, L.; Smith, B.; Moverare, J.J. Improved fatigue strength of additively manufactured Ti6Al4V by surface post processing. *Int. J. Fatigue* **2020**, 134, 105497.
10. Kuji, C.; Soyama, H. Mechanical surface treatment of titanium alloy Ti6Al4V manufactured by direct metal laser sintering using laser cavitation. *Metals* **2023**, 13, 181.
11. Sano, Y.; Obata, M.; Kubo, T.; Mukai, N.; Yoda, M.; Masaki, K.; Ochi, Y. Retardation of crack initiation and growth in austenitic stainless steels by laser peening without protective coating. *Mater. Sci. Eng. A* **2006**, 417, 334-340.
12. Mao, B.; Siddaiah, A.; Menezes, P.L.; Liao, Y.L. Surface texturing by indirect laser shock surface patterning for manipulated friction coefficient. *J. Mater. Process. Technol.* **2018**, 257, 227-233.
13. Kawashima, T.; Sano, T.; Hirose, A.; Tsutsumi, S.; Masaki, K.; Arakawa, K.; Hori, H. Femtosecond laser peening of friction stir welded 7075-T73 aluminum alloys. *J. Mater. Process. Technol.* **2018**, 262, 111-122.
14. Yoshida, M.; Nishibata, I.; Matsuda, T.; Ito, Y.; Sugita, N.; Shiro, A.; Shobu, T.; Arakawa, K.; Hirose, A.; Sano, T. Influence of pulse duration on mechanical properties and dislocation density of dry laser peened aluminum alloy using ultrashort pulsed laser-driven shock wave. *J. Appl. Phys.* **2022**, 132,
15. Sano, Y.; Akita, K.; Sano, T. A mechanism for inducing compressive residual stresses on a surface by laser peening without coating. *Metals* **2020**, 10, 816.
16. Soyama, H. Laser cavitation peening and its application for improving the fatigue strength of welded parts. *Metals* **2021**, 11, 531.
17. Gu, J.Y.; Luo, C.H.; Ma, P.C.A.; Xu, X.C.; Wu, Y.; Ren, X.D. Study on processing and strengthening mechanisms of mild steel subjected to laser cavitation peening. *Appl. Surf. Sci.* **2021**, 562, 150242.
18. Sasoh, A.; Watanabe, K.; Sano, Y.; Mukai, N. Behavior of bubbles induced by the interaction of a laser pulse with a metal plate in water. *Appl. Phys. A* **2005**, 80, 1497-1500.
19. Soyama, H. Key factors and applications of cavitation peening. *Inter. J. Peen. Sci. Technol.* **2017**, 1, 3-60.
20. Soyama, H. Comparison between the improvements made to the fatigue strength of stainless steel by cavitation peening, water jet peening, shot peening and laser peening. *J. Mater. Process. Technol.* **2019**, 269, 65-78.
21. Soyama, H.; Sekine, Y.; Saito, K. Evaluation of the enhanced cavitation impact energy using a pvdf transducer with an acrylic resin backing. *Measurement* **2011**, 44, 1279-1283.
22. Glaser, D.; Polese, C. Cavitation bubble oscillation period as a process diagnostic during the laser shock peening process. *Appl. Phys. A* **2017**, 123, 603.

23. Ren, X.D.; Wang, J.; Yuan, S.Q.; Adu-Gyamfi, S.; Tong, Y.Q.; Zuo, C.Y.; Zhang, H.F. Mechanical effect of laser-induced cavitation bubble of 2a02 alloy. *Opt. Laser Technol.* **2018**, *105*, 180-184.
24. Saitou, N.; Enomoto, K.; Kurosawa, K.; Morinaka, R.; Hayashi, E.; Ishikwa, T.; Yoshimura, T. Development of water jet peening technique for reactor internal components of nuclear power plant. *J. Jet Flow Eng.* **2003**, *20*, No. 1, 4-12.
25. Soyama, H. Cavitating jet: A review. *Applied Sciences* **2020**, *10*, 1-27.
26. Plesset, M.S.; Chapman, R.B. Collapse of an initially spherical vapour cavity in neighbourhood of a solid boundary. *J. Fluid Mech.* **1971**, *47*, 283-290.
27. Lauterborn, W.; Bolle, H. Experimental investigations of cavitation-bubble collapse in neighborhood of a solid boundary. *J. Fluid Mech.* **1975**, *72*, 391-399.
28. Crum, L.A. Surface oscillations and jet development in pulsating bubbles. *J. de Phys. Colloques* **1979**, *40*, 285-288.
29. Brennen, C.E., Cavitation and bubble dynamics, Oxford University Press, **1995**.
30. Ley, S.V.; Low, C.M.R., Ultrasound in synthesis, Springer-Verlag, Berlin, **1980**.
31. Gonzalez-Avila, S.R.; Denner, F.; Ohl, C.-D. The acoustic pressure generated by the cavitation bubble expansion and collapse near a rigid wall. *Phys. Fluids* **2021**, *33*, 032118.
32. Park, S.-H.; Phan, T.-H.; Park, W.-G. Numerical investigation of laser-induced cavitation bubble dynamics near a rigid surface based on three-dimensional fully compressible model. *Inter. J. Heat and Mass Transfer* **2022**, *191*, 122853.
33. Sun, Y.; Du, Y.; Yao, Z.; Zhong, Q.; Geng, S.; Wang, F. The effect of surface geometry of solid wall on the collapse of a cavitation bubble. *J. Fluids Eng.* **2022**, *144*, 071402.
34. Sieber, A.B.; Preso, D.B.; Farhat, M. Cavitation bubble dynamics and microjet atomization near tissue-mimicking materials. *Phys. Fluids* **2023**, *35*, 027101.
35. Iga, Y.; Sasaki, H. Relationship between a non-spherical collapse of a bubble and a stress state inside a wall. *Phys. Fluids* **2023**, *35*, 023312.
36. Hatamleh, O.; Lyons, J.; Forman, R. Laser and shot peening effects on fatigue crack growth in friction stir welded 7075-T7351 aluminum alloy joints. *Int. J. Fatigue* **2007**, *29*, 421-434.
37. Gill, A.; Telang, A.; Mannava, S.R.; Qian, D.; Pyoun, Y.-S.; Soyama, H.; Vasudevan, V.K. Comparison of mechanisms of advanced mechanical surface treatments in nickel-based superalloy. *Mater. Sci. Eng. A* **2013**, *576*, 346-355.
38. Philipp, A.; Lauterborn, W. Cavitation erosion by single laser-produced bubbles. *J. Fluid Mech.* **1998**, *361*, 75-116.
39. Soyama, H. Introduction of compressive residual stress into alloy tool steel by submerged laser peening utilizing laser cavitation impact. *Proc. 9th Inter. Conf. Leading Edge Manufacturing in 21st Century, LEM 2017* **2017**, 010.
40. Sano, Y.; Kato, T.; Mizuta, Y.; Tamaki, S.; Yokofujita, K.; Taira, T.; Hosokai, T.; Sakino, Y. Development of a portable laser peening device and its effect on the fatigue properties of HT780 butt-welded joints. *Forces in Mechanics* **2022**, *7*, 100080.
41. Kang, C.; Liu, H.X.; Soyama, H. Estimation of aggressive intensity of a cavitating jet with multiple experimental methods. *Wear* **2018**, *394*, 176-186.
42. Noor Shahira Masroon, N.S.; Hirata, H.; Tsuyama, M.; Heya, M.; Nakano, H. Effects of laser peening parameters on plastic deformation in aqueous glycerol solution as plasma confinement layer. *J. Laser Micro/Nanoengineering* **2021**, *16*, 160-165.
43. Soyama, H.; Kokubun, T. Effect of impact induced by cavitation bubble on submerged laser peening. *J. Shot Peening Technol. Japan* **2016**, *28*, 48-49.
44. J442 Test strip, holder, and gage for shot peening. *SAE Inter. Standards* **2013**, 1-5.
45. J443 Procedures for using standard shot peening almen strip. *SAE Inter. Standards* **2010**, 1-6.
46. Soyama, H. Cavitation peening: A review. *Metals* **2020**, *10*, 270.
47. Soyama, H. Comparison between impact induced by abrasion and bubble collapse impact on laser peening. *Proc. Mechanics Engineering Congress* **2016**, 16-1, G0400402.
48. Soyama, H.; Yahata, Y.; Saito, M. Aspect of bubbles in narrow tube imitating root canal induced by er:Yag laser. *Proc. 11th Inter. Sympo. Cavitation* **2021**, 229-232.
49. Sugimoto, Y.; Obata, S. Behavior of a sphere caused by pulsed laser induced bubble simulating stone crushing with tul. *Proc. 11th Inter. Sympo. Cavitation* **2021**, 614-617.



50. Nguyen, T.T.P.; Tanabe, R.; Ito, Y. Influences of focusing conditions on dynamics of laser ablation at a solid–liquid interface. *Applied Physics Express* **2013**, *6*, 1–4.
51. Soyama, H. Comparison between shot peening, cavitation peening and laser peening by observation of crack initiation and crack growth in stainless steel. *Metals* **2020**, *10*, 63.
52. Lauterborn, W.; Ohl, C.D. Cavitation bubble dynamics. *Ultrason. Sonochem.* **1997**, *4*, 65–75.
53. Ohl, C.D.; Lindau, O.; Lauterborn, W. Luminescence from spherically and aspherically collapsing laser induced bubbles. *Phys. Rev. Lett.* **1998**, *80*, 393–396.
54. Ohl, C.D.; Kurz, T.; Geisler, R.; Lindau, O.; Lauterborn, W. Bubble dynamics, shock waves and sonoluminescence. *Philos. Trans. R. Soc. A* **1999**, *357*, 269–294.
55. Soyama, H. Luminescence intensity of vortex cavitation in a venturi tube changing with cavitation number. *Ultrason. Sonochem.* **2021**, *71*, 105389.
56. Rayleigh, L. On the pressure developed in a liquid during the collapse of a spherical cavity. *The London, Edinburgh, and Dublin Philosophical Magazine and Journal of Science* **1917**, *34*, 94–98.
57. Soyama, H.; Kuji, C.; Kuriyagawa, T.; Chighizola, C.R.; Hill, M.R. Optimization of residual stress measurement conditions for a 2D method using X-ray diffraction and its application for stainless steel treated by laser cavitation peening. *Materials* **2021**, *14*, 2772.
58. Soyama, H. Surface mechanics design by cavitation peening using submerged pulse laser. *Abstracts of 7th Inter. Conf. Laser Peening and Related Phenomena* **2018**, 57.
59. Soyama, H. Introduction of compressive residual stress into stainless steel by bubble induced by submerged pulse laser. *J. Shot Peening Technol. Japan* **2019**, *31*, 86–87.
60. Soyama, H.; Kuji, C. Improving effects of cavitation peening, using a pulsed laser or a cavitating jet, and shot peening on the fatigue properties of additively manufactured titanium alloy Ti6Al4V. *Surf. Coat. Technol.* **2022**, 451, 129047.
61. Little, R.E. Estimating the median fatigue limit for very small up-and-down quantal response tests and for S-N data with runouts. *ASTM STP* **1972**, 511, 29–42.
62. Kumagai, M.; Curd, M.E.; Soyama, H.; Ungár, T.; Ribárik, G.; Withers, P.J. Depth-profiling of residual stress and microstructure for austenitic stainless steel surface treated by cavitation, shot and laser peening. *Mater. Sci. Eng. A* **2021**, *813*, 141037.
63. Soyama, H.; Takeo, F. Effect of various peening methods on the fatigue properties of titanium alloy Ti6Al4V manufactured by direct metal laser sintering and electron beam melting. *Materials* **2020**, *13*, 2216.
64. Soyama, H.; Kuji, C. Comparison on fatigue strength of additive manufactured titanium alloy by various peening methods. *Proc. Annual Meeting Soc. Mater. Sci., Japan* **2023**, 72.
65. Soyama, H. Improvement of fatigue properties of magnesium alloy by cavitation peening using a submerged water jet and a pulse laser. *Metal Finishing News* **2021**, *22*, 56–59.
66. Munoz-Cubillos, J.; Coronado, J.J.; Rodriguez, S.A. Deep rolling effect on fatigue behavior of austenitic stainless steels. *Int. J. Fatigue* **2017**, *95*, 120–131.
67. Zhou, J.; Retraint, D.; Sun, Z.; Kanoute, P. Comparative study of the effects of surface mechanical attrition treatment and conventional shot peening on low cycle fatigue of a 316L stainless steel. *Surf. Coat. Technol.* **2018**, *349*, 556–566.
68. Telang, A.; Gnaupel-Herold, T.; Gill, A.; Vasudevan, V.K. Effect of applied stress and temperature on residual stresses induced by peening surface treatments in alloy J. *Mater. Eng. Perform.* **2018**, *27*, 2796–2804.
69. Ben Moussa, N.; Gharbi, K.; Chaieb, I.; Ben Fredj, N. Improvement of AISI 304 austenitic stainless steel low-cycle fatigue life by initial and intermittent deep rolling. *Int. J. Adv. Manuf. Technol.* **2019**, *101*, 435–449.
70. Yang, S.; Zeng, W.; Yang, J. Characterization of shot peening properties and modelling on the fatigue performance of 304 austenitic stainless steel. *Int. J. Fatigue* **2020**, *137*, 105621.
71. Soyama, H.; Chighizola, C.R.; Hill, M.R. Effect of compressive residual stress introduced by cavitation peening and shot peening on the improvement of fatigue strength of stainless steel. *J. Mater. Process. Technol.* **2021**, *288*, 116877.
72. Soyama, H. Laser cavitation peening using a Nd:YAG laser with and without Q-switch. *Abstracts of Quantum Beam Application for Sciences and Industries* **2023**, 51.

**Disclaimer/Publisher's Note:** The statements, opinions and data contained in all publications are solely those of the individual author(s) and contributor(s) and not of MDPI and/or the editor(s). MDPI and/or the editor(s) disclaim responsibility for any injury to people or property resulting from any ideas, methods, instructions or products referred to in the contents.